J. Eur. Opt. Society-Rapid Publ. 2024, **20**, 14

https://doi.org/10.1051/jeos/2024012
Available online at: https://jeos.edpsciences.org

Journal of the European Optical Society-Rapid Publications

Special Issue - Plasmonica 2023
Antonino Foti and Attilio Zilli (Guest editors)

SHORT COMMUNICATION OPEN ACCESS

Germanium Fabry-Perot nanoresonators investigated by cathodoluminescence spectroscopy

Sandro Mignuzzi[1], Xiaofei Wu[2], Bert Hecht[2], Jacopo Frigerio[3], Giovanni Isella[3], Michele Celebrano[4], Marco Finazzi[4], Riccardo Sapienza[1], and Paolo Biagioni[4,*]

[1] Blackett Laboratory, Department of Physics, Imperial College London, Prince Consort Rd, London SW7 2BW, United Kingdom
[2] Nano-optics and Biophotonics Group, Experimental Physics 5, Institute of Physics, University of Würzburg, Am Hubland, 97074 Würzburg, Germany
[3] L-NESS, Dipartimento di Fisica, Politecnico di Milano, Polo di Como, Via Anzani 42, 22100 Como, Italy
[4] Dipartimento di Fisica, Politecnico di Milano, Piazza Leonardo da Vinci 32, 20133 Milano, Italy

Received 11 January 2024 / Accepted 16 March 2024

Abstract. We report on the experimental investigation, by means of spatially-resolved cathodoluminescence spectroscopy, of rectangular all-dielectric Ge nanoantennas sustaining Fabry-Perot resonances. The combination of spatial and spectral resolution allows us to directly image the standing-wave pattern of the local density of optical states inside the nanoantennas, which is the fingerprint of the resonant Purcell contribution to the overall emission enhancement previously reported in the literature for the same structures. Our results confirm that the emission properties of Ge nanostructures can be effectively tuned by engineering the local density of optical states and that cathodoluminescence provides valuable information to experimentally address such modulation in their emission properties.

Keywords: Dielectric nanoantennas, Cathodoluminesce spectroscopy, Germanium.

All-dielectric nanoresonators operating in the visible and near-infrared spectral range have become a crucial ingredient for the enhancement of light-matter interactions at the nanoscale, since they combine a large local density of optical states with negligible absorption losses [1–3]. High-index, undoped semiconducting materials have been employed to realize dielectric nanoantennas, often in the form of individual disks or cylinders that support a rich variety of Mie resonances [4–8]. Many other geometries have also been explored, such as disk dimers [9–11], hollow structures [7, 12, 13], nanowires [14], or nanoscale truncated waveguides supporting Fabry-Perot resonances [15–18].

The optical characterization of individual dielectric nanoantennas typically relies on confocal microscopy, exploiting either elastic scattering [4, 14, 16], photoluminescence from the antenna material [15], nonlinear effects [5–7, 10], or the coupling with photon emitters [7, 9, 11, 19]. However, diffraction-limited optical techniques do not allow resolving the spatial features of the resonant field distribution inside the dielectric nanoantennas. To this aim, both near-field microscopy [18, 20, 21] and scanning-electron cathodoluminescence microscopy [22–24] have been applied. Specifically, apertureless near-field microscopy is mostly sensitive to the out-of-plane component (along the tip axis) of the local electric field outside the nanoantenna, which is efficiently scattered by the tip, while cathodoluminescence relies on the broadband generation of photons when a fast electron impinges onto a surface. Such an interaction can be effectively described as giving rise to a point-like emitting dipole, which makes spatially-resolved cathodoluminescence the ideal tool to experimentally address the local density of photonic states inside the nanoantenna [25–27].

Ge nanoantennas fabricated on Si in the form of rectangular nanoscale waveguide resonators already demonstrated an almost 30-fold enhancement in the collected spontaneous emission per unit volume compared to a continuous Ge film [15]. The Purcell contribution (reduction of the excited-state lifetime) to such enhancement, in particular, was analyzed with finite-difference time-domain simulations and attributed to the presence of Fabry-Perot resonances for the fundamental transverse-electric (TE) and transverse-magnetic (TM) modes supported by the nanoantennas. Yet, only indirect evidence was provided about this explanation, *i.e.* the measured enhancement of the Ge direct-gap emission as a function of the antenna length.

* Corresponding author: paolo.biagioni@polimi.it

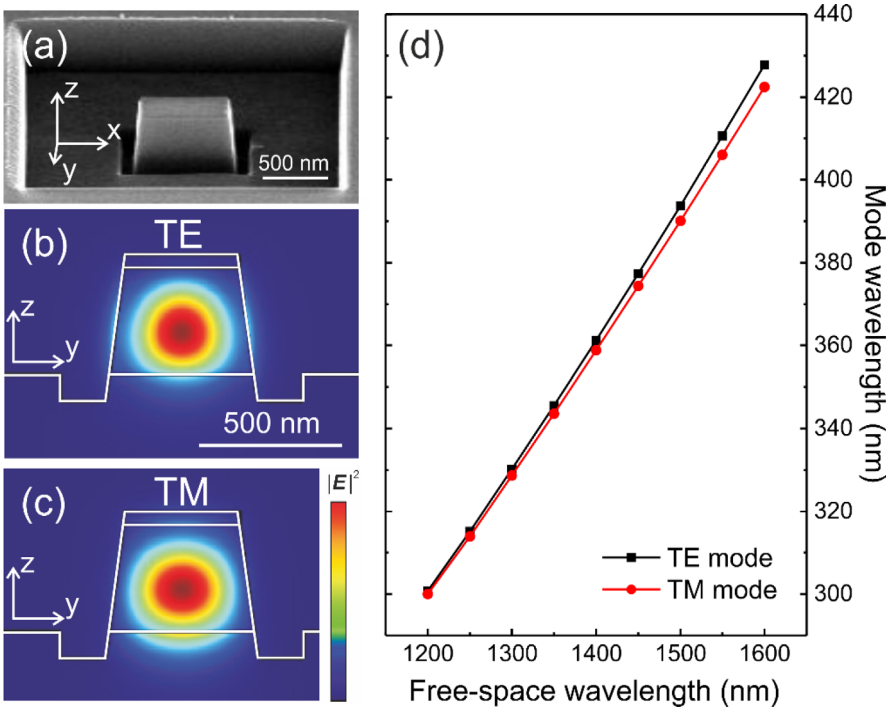

Fig. 1. Investigated Ge nanoantennas: (a) representative scanning electron microscopy image; (b, c) intensity profile of the fundamental TE and TM modes, respectively, simulated employing the mode source in the FDTD Ansys Lumerical software; (d) dispersion relations (mode wavelength as a function of the free-space wavelength) for the fundamental TE and TM modes.

In this work, we provide direct evidence of Fabry-Perot standing waves in such Ge nanoantennas exploiting cathodoluminescence microscopy. By doing so, we demonstrate that a standing wave is indeed clearly visible along the nanoresonator when the resonance conditions are met. The effective index of the mode and its associated wavelength, as extracted from the experimental maps, are in very good agreement with the numerical predictions and confirm that the field enhancement in the investigated nanostructures can be partially attributed to Fabry-Perot resonances of the truncated waveguide.

The sample under investigation was fabricated by focused ion-beam milling employing Ga ions, starting from a 400-nm-thick heavily-doped Ge film grown on a standard Si(001) wafer by low-energy plasma-enhanced chemical vapor deposition (doping concentration around 10^{19} cm^{-3}) [28]. Each antenna can be described as a truncated waveguide with a fixed cross-section of about 400 × 400 nm^2 and varying length. A representative scanning electron microscopy image shown in Figure 1a points out that the actual nanostructure geometry presents tilted side walls and a slight undercut into the Si substrate around the milled antenna. All these features are accounted for in the numerical simulations. Moreover, the antenna is covered with a 50-nm-thick silicon oxide film, which is functional to increase the quality of the ion-beam milling, as discussed in references [15].

The cross section of the nanoresonator is designed so that only two almost-degenerate fundamental modes are sustained, with a dominant TE and TM character, respectively. Their intensity profiles on a plane coinciding with the transverse cross section of the antenna, simulated with the mode solver of the FDTD Ansys Lumerical software, are shown in Figures 1b and 1c, along with their dispersion relations (*i.e.* mode wavelength as a function of the free-space wavelength, see Fig. 1d).

In the setup employed for this work, cathodoluminescence is excited by a 30-keV electron beam inside a scanning electron microscope and is collected by a parabolic mirror (0.98 numerical aperture) that collimates the emitted radiation and redirects it through an optical collection system directly onto an InGaAs spectrometer, without the use of any optical fiber [23]. The experimental analysis is performed on the total intensity impinging onto the detector, with no sensitivity to the polarization state of the emitted light. We focus our analysis on an individual nanoantenna with a length of 1400 nm, as shown in the top-view scanning electron microscopy image of Figure 2a. The cathodoluminescence spectrum is acquired as a function of the position of the electron beam along the main antenna axis. The resulting two-dimensional map, representing the collected intensity as a function of the wavelength and the beam position, is reported in Figure 2b. A quick inspection of the map clearly reveals that, for specific wavelengths, a standing-wave pattern is visible inside the nanoantenna, which points to the occurrence of Fabry-Perot resonances modulating the local density of optical states available for the radiative decay of the emission dipoles. Such resonances are generated by the constructive interference of the two degenerate guided modes bouncing back and forth inside the truncated waveguide, thanks to the reflectivity of the end facets. They occur for antenna lengths that are equal

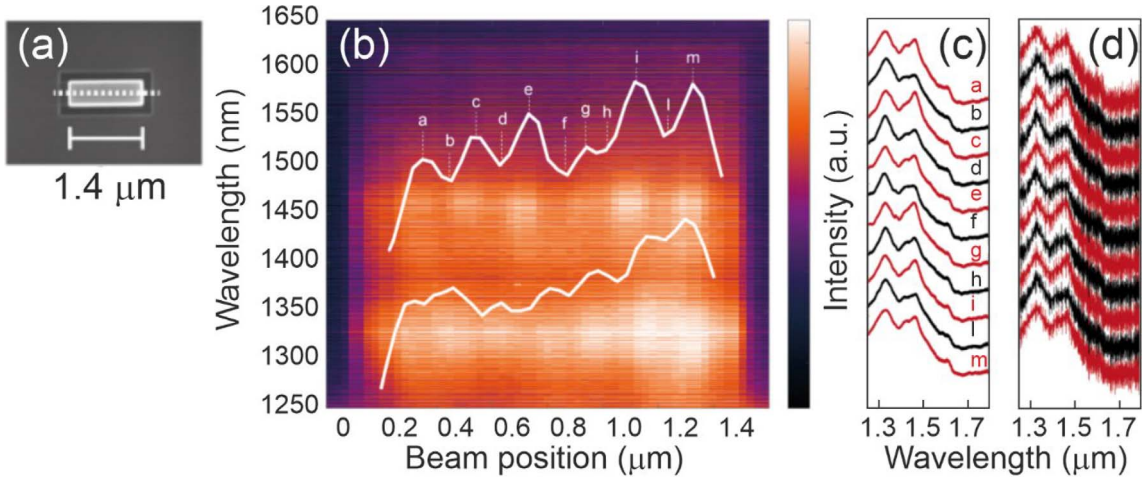

Fig. 2. Cathodoluminescence investigation of the Ge nanoantenna: (a) top-view scanning electron microscopy images of the investigated nanoantenna (the dashed line represents the trajectory of the scanning electron beam during the acquisition of the cathodoluminescence spectra); (b) two-dimensional map (emission wavelength as a function of the electron beam position along the antenna axis) from the cathodoluminescence investigation, with solid white lines representing the intensity profile integrated over a wavelength range of about 50 nm around each resonance; (c) smoothened cathodoluminescence spectra acquired at specific positions (marked with letters a-m on panel b) along the antenna axis, after vertical translation for sake of readability; (d) raw data for the smoothened cathodoluminescence spectra of panel c.

to a multiple of half the mode wavelength. In practice, the transition dipole generated by the keV electrons impinging onto the antenna can radiatively decay into the Fabry-Perot modes of the nanocavity. This mechanism determines a spatially-dependent decay rate, which reflects in the collected intensity signal. By averaging the spatially- and frequency-resolved signal over a wavelength range of about 50 nm around the two resonant wavelengths observed experimentally in Figure 2b, the white solid lines superimposed to the map are obtained, which allow for a more quantitative analysis of the phenomenon.

Evidence for the observed resonances is also provided by individual cathodoluminescence spectra in Figures 2c and 2d, which are acquired at specific locations along the antenna axis, as marked by the letters a–m in Figure 2b. Two peaks around 1330 nm and 1460 nm are clearly visible, corresponding to the central wavelengths of the standing-wave patterns in the map of Figure 2b.

To analyze and interpret the experimental findings, let us recall that the fundamental TE and TM modes in the truncated Ge waveguide are practically degenerate. As a result, they possess roughly the same mode wavelength, while higher order modes are not supported by the small cross section of the waveguide [15]. We expect that the standing-wave patterns imaged by the cathodoluminescence setup present a well-defined spatial periodicity of half the mode wavelength at the specific resonance frequency. Such a spatial periodicity can be easily evaluated by measuring the approximate distance between the outer intensity peaks in the standing-wave pattern and dividing by the number of the periods. By doing so, we find mode wavelengths of about 335 nm and 390 nm for the two resonance peaks. These experimental results are in excellent agreement with the simulations reported in Figure 1d, which predict mode wavelengths of about 338 nm and 380 nm for the same free-space wavelengths of 1330 nm and 1460 nm, respectively. Interestingly, the non-trivial lineshapes of the two main peaks in Figures 2c and 2d might be a hint of the non-perfect degeneracy of the TE and TM modes involved in the resonant emission process. It should also be noted, for sake of completeness, that for the two investigated resonances we observe 6 and 7 intensity maxima inside the antenna, *i.e.* we have evidence for Fabry-Perot modes in which the cavity length is 6 or 7 times the half mode wavelength, respectively. This would point to an expected cavity length of about 1350 nm sustaining such resonances. Indeed, the estimate of a nominal length of 1400 nm for the footprint of the investigated nanostructure does not take into account the presence of tilted side walls for the reflecting end facets, which results in a shorter effective length as demonstrated experimentally.

In conclusion, we employed spatially-resolved cathodoluminescence spectroscopy in a scanning electron microscope coupled to an optical spectrograph to provide direct experimental evidence of the presence of Fabry-Perot resonances in rectangular Ge nanoantennas. The investigation allows imaging the standing-wave pattern of the local density of optical states inside the nanoantenna and confirms that cathodoluminescence represents a key asset in the engineering of nanophotonic devices and in the experimental assessment of their performance. Perspective combinations of this technique with electron energy-loss spectroscopy might further enrich the information, leveraging the possibility to discriminate between local density of states and radiative local density of states and possibly also between TE and TM modes [29].

Funding

Funding from *Fondazione Cariplo* under the project "Nano antennas of germanium for advanced photonics (NANOGAP)" (project number 2010-0632) is gratefully acknowledged.

Conflicts of Interest

The authors declare that they have no competing interests to report.

Data availability statement

The data associated with this study is available upon request. Please contact the corresponding author to request access to the data.

Author contribution statement

All authors actively contributed to the design of the experiment, the discussion of the results, and the preparation of the manuscript. S.M. and R.S. performed the cathodoluminescence measurements. X.W., B.H., J.F., and G.I. performed the growth and nanofabrication of the Ge nanoantenna. M.C., M.F., and P.B. performed the numerical modeling.

References

1 Decker M., Staude I. (2016) Resonant dielectric nanostructures: a low-loss platform for functional nanophotonics, *J. Opt.* **18**, 103001.
2 Kuznetsov A.I., Miroshnichenko A.E., Brongersma M.L., Kivshar Y. S., Luk'yanchuk B. (2016) Optically resonant dielectric nanostructures, *Science* **354**, aag2472.
3 Alhalabya H., Zaraket H., Principe M. (2021) Enhanced photoluminescence with dielectric nanostructures: a review, *Results Opt.* **3**, 100073.
4 Staude I., Miroshnichenko A.E., Decker M., Fofang N.T., Liu S., Gonzales E., Dominguez J., Luk T.S., Neshev D.N., Brener I., Kivshar Y. (2013) Tailoring directional scattering through magnetic and electric resonances in subwavelength silicon nanodisks, *ACS Nano* **7**, 7824–7832.
5 Gili V.F., Carletti L., Locatelli A., Rocco D., Finazzi M., Ghirardini L., Favero I., Gomez C., Lemaître A., Celebrano M., De Angelis C., Leo G. (2016) Monolithic AlGaAs second-harmonic nanoantennas, *Opt. Exp.* **24**, 15965–15971.
6 Grinblat G., Li Y., Nielsen M.P., Oulton R.F., Maier S.A. (2017) Efficient third harmonic generation and nonlinear subwavelength imaging at a higher-order anapole mode in a single germanium nanodisk, *ACS Nano* **11**, 953–960.
7 Cambiasso J., Grinblat G., Li Y., Rakovich A., Cortés E., Maier S.A. (2017) Bridging the gap between dielectric nanophotonics and the visible regime with effectively lossless gallium phosphide antennas, *Nano Lett.* **17**, 1219–1225.
8 Capretti A., Lesage A., Gregorkiewicz T. (2017) Integrating quantum dots and dielectric Mie resonators: a hierarchical metamaterial inheriting the best of both, *ACS Photonics* **4**, 2187–2196.
9 Regmi R., Berthelot J., Winkler P.M., Mivelle M., Proust J., Bedu F., Ozerov I., Begou T., Lumeau J., Rigneault H., García-Parajó M.F., Bidault S., Wenger J., Bonod N. (2016) All-dielectric silicon nanogap antennas to enhance the fluorescence of single molecules, *Nano Lett.* **16**8, 5143–5151.
10 Carletti L., Rocco D., Locatelli A., De Angelis C., Gili V.F., Ravaro M., Favero I., Leo G., Finazzi M., Ghirardini L., Celebrano M., Marino G., Zayats A.V. (2017) Controlling second-harmonic generation at the nanoscale with monolithic AlGaAs-on-AlOx antennas, *Nanotechnology* **28**, 114005.
11 Sortino L., Zotev P.G., Phillips C.L., Brash A.J., Cambiasso J., Marensi E., Fox A.M., Maier S.A., Sapienza R., Tartakovskii A.I. (2021) Bright single photon emitters with enhanced quantum efficiency in a two-dimensional semiconductor coupled with dielectric nano-antennas, *Nature Comm.* **12**, 6063.
12 Yang Y., Zenin V.A., Bozhevolnyi S.I. (2018) Anapole-assisted strong field enhancement in individual all-dielectric nanostructures, *ACS Photonics* **5**, 1960–1966.
13 Mignuzzi S., Vezzoli S., Horsley S.A., Barnes W.L., Maier S.A., Sapienza R. (2019) Nanoscale design of the local density of optical states, *Nano Lett.* **19**, 1613–1617.
14 Cao L., Fan P., Barnard E.S., Brown A.M., Brongersma M.L. (2010) Tuning the color of silicon nanostructures, *Nano Lett.* **10**, 2649–2654.
15 Celebrano M., Baselli M., Bollani M., Frigerio J., Bahgat Shehata A., Della Frera A., Tosi A., Farina A., Pezzoli F., Osmond J., Wu X., Hecht B., Sordan R., Chrastina D., Isella G., Duò L., Finazzi M., Biagioni P. (2015) Emission engineering in germanium nanoresonators, *ACS Photonics* **2**, 53–59.
16 Ee H.S., Kang J.H., Brongersma M.L., Seo M.K. (2015) Shape-dependent light scattering properties of subwavelength silicon nanoblocks, *Nano Lett.* **15**, 1759–1765.
17 Landreman P.E., Chalabi H., Park J., Brongersma M.L. (2016) Fabry-Perot description for Mie resonances of rectangular dielectric nanowire optical resonators, *Opt. Exp.* **24**, 29760–29772.
18 Frolov A.Y., Verellen N., Li J., Zheng X., Paddubrouskaya H., Denkova D., Shcherbakov M.R., Vandenbosch G.A.E., Panov V.I., Van Dorpe P., Fedyanin A.A., Moshchalkov V.V. (2017) Near-field mapping of optical Fabry-Perot modes in all-dielectric nanoantennas, *Nano Lett.* **17**, 7629–7637.
19 Córdova-Castro R.M., van Dam B., Lauri A., Maier S.A., Sapienza R., De Wilde Y., Izeddin I., Krachmalnicoff V. (2024) Single-emitter super-resolved imaging of radiative decay rate enhancement in dielectric gap nanoantennas, *Light Sci. App.* **13**, 7.
20 Bakker R.M., Permyakov D., Yu Y.F., Markovich D., Paniagua-Domínguez R., Gonzaga L., Samusev A., Kivshar Y., Luk'yanchuk B., Kuznetsov A.I. (2015) Magnetic and electric hotspots with silicon nanodimers, *Nano Lett.* **15**, 2137–2142.
21 Granchi N., Montanari M., Ristori A., Khoury M., Bouabdellaoui M., Barri C., Fagiani L., Gurioli M., Bollani M., Abbarchi M., Intonti F. (2021) Near-field hyper-spectral imaging of resonant Mie modes in a dielectric island, *APL Photonics* **6**, 126102.
22 Mignuzzi S., Mota M., Coenen T., Li Y., Mihai A.P., Petrov P.K., Oulton R.F.M., Maier S.A., Sapienza R. (2018) Energy-momentum cathodoluminescence spectroscopy of dielectric nanostructures, *ACS Photonics* **5**, 1381–1387.
23 Sapienza R., Coenen T., Renger J., Kuttge M., van Hulst N.F., Polman A. (2012) Deep-subwavelength imaging of the modal dispersion of light, *Nat. Mat.* **11**, 781–787.
24 Dang Z., Chen Y., Fang Z. (2023) Cathodoluminescence nanoscopy: state of the art and beyond, *ACS Nano* **17**, 24431–24448.
25 Coenen T., van de Groep J., Polman A. (2013) Resonant modes of single silicon nanocavities excited by electron irradiation, *ACS Nano.* **7**, 1689–1698.
26 Polman A., Kociak M., García de Abajo F.J. (2019) Electron-beam spectroscopy for nanophotonics, *Nat. Mat.* **18**, 1158–1171.
27 Dong Z., Mahfoud Z., Paniagua-Domínguez R., Wang H., Fernández-Domínguez A.I., Gorelik S., Ha S.T., Tjiptoharsono F., Kuznetsov A. I., Bosman M., Yang J.K.W. (2022) Nanoscale mapping of optically inaccessible bound-states-in-the-continuum, *Light Sci. App.* **11**, 20.
28 Frigerio J., Ballabio A., Isella G., Sakat E., Pellegrini G., Biagioni P., Bollani M., Napolitani E., Manganelli C., Virgilio M., Grupp A., Fischer M.P., Brida D., Gallacher K., Paul D.J., Baldassarre L., Calvani P., Giliberti V., Nucara A., Ortolani M. (2016) Tunability of the dielectric function of heavily doped germanium thin films for mid-infrared plasmonics, *Phys. Rev. B* **94**, 085202.
29 Auad Y., Hamon C., Tencé M., Lourenço-Martins H., Mkhitaryan V., Stéphan O., Garcia de Abajo F.J., Tizei L.H., Kociak M. (2022) Unveiling the coupling of single metallic nanoparticles to whispering-gallery microcavities, *Nano Lett.* **22**, 319–327.